PCCP

Localized Electronic and Vibrational States in Amorphous Diamond

Journal:	*Physical Chemistry Chemical Physics*
Manuscript ID	CP-ART-12-2020-006393.R1
Article Type:	Paper
Date Submitted by the Author:	23-Jan-2021

Complete List of Authors:	Cheng, Rong; Qingdao University, College of physics Lu, Wen-Cai; Qingdao University, College of physics Ho, Kai Ming; Iowa State University, Ames Laboratory-U.S. DOE and Department of Physics and Astronomy Wang, Cai Zhuang; Iowa State University, Ames Laboratory-U.S. DOE and Department of Physics and Astronomy

Localized Electronic and Vibrational States in Amorphous Diamond

Rong Cheng,[1,2] Wen-Cai Lu,[1,2] K. M. Ho[2] and C. Z. Wang[2†]

[1]*College of Physics, Qingdao University, Qingdao, Shandong 266071, China*
[2]*Ames Laboratory-U.S. DOE and Department of Physics and Astronomy, Iowa State University, Ames, IA 50011, U.S.A*

Abstract

Amorphous diamond structures are generated by quenching high-density high-temperature liquid carbon using tight-binding molecular-dynamics simulations. We show that the generated amorphous diamond structures are predominated by strong tetrahedral bonds with the sp^3 bonding fraction as high as 97%, thus exhibit an ultra-high incompressibility and wide band gap close to those of crystalline diamond. A small amount of sp^2 bonding defects in the amorphous sample contributes to localized electronic states in the band gap while large local strain gives rise to localization of vibrational modes at both high and low frequency regimes.

I. Introduction

As an important class of noncrystalline solids, covalently bounded amorphous semiconductors have attracted considerable interests in both fundamental research and technological applications. While amorphous silicon (*a-Si*) has been studied extensively in the past several decades and has found widespread applications in microelectronics and photovoltaic industries, amorphous diamond (*a-Dia*) with tetrahedral bonding topology similar to that of *a-Si* has been synthesized only very recently [1]. Using a combination of high pressure and *in situ* laser heating techniques, Zeng *et al*. have reported the synthesis of bulk quenchable *a-Dia* from glassy carbon [1]. The sp^3 bonding fraction of the *a-Dia* is reported to be close to 98% and the density of the samples is estimated to be 3.3 ± 0.1 g/cm^3, close to that of crystalline diamond (3.52 g/cm^3). The *a-Dia* is also shown to be optically transparent and has ultrahigh incompressibility (i.e., large bulk modulus) comparable to that of crystalline diamond.

While amorphous carbon (*a-C*) materials with various bonding topologies (i.e., different sp^2/sp^3 bonding ratios) have been intensively investigated over the past several decades [2-17], most of those so called "diamond-like" *a-C* obtained from experimental synthesis still have high fraction (about 15%) of sp^2 bonding atoms [3-5]. The properties of the diamond-like *a-C* with such high fraction of sp^2 bonding sites would be very different from the *a-Dia* with close to 100% of tetrahedral bonding topology. Although some *a-Dia* structure with over 95% of sp^3 bonding sites generated by computer simulations have been reported in the literature, detailed analysis of the properties of such *a-Dia*

models are still lacking [17]. To evaluate further the potential applications of this new allotrope of carbon, insights into the structure and properties of *a-Dia* at the atomic and electronic levels are highly desirable.

In this paper, we investigate the atomic structures as well as the electronic and vibrational properties of *a-Dia,* focusing on the mechanisms of the localization of the electronic states caused by the sp^2 defects and the vibrational states produced by the structural distortions in the *a-Dia*. High-quality atomistic structure models of *a-Dia* are generated using efficient and accurate of tight-binding molecular dynamics (TBMD) simulations, based on which the structural, electronic and vibrational properties are analyzed and predicted. We show that the *a-Dia* structures generated by our TBMD simulations have as high as 97% of sp^3 bonding fraction. The generated *a-Dia* samples also exhibit ultra-high incompressibility with their bulk moduli reaching about 87% of the bulk modulus of crystalline diamond. We show that the generated *a-Dia* samples also have a wide band gap similar to that of diamond except some defect states in the gap. These gap states are well localized on the 3-fold coordinated carbon atoms. We also find that large local strain in the *a-Dia* network produces well localized vibrational modes which would have significant effects on the thermal conductivity of the material.

II. Calculation Methods

TBMD simulations are performed using a recently developed three-center (3c) TB potential for carbon [18]. The TB potential retains sufficient quantum mechanics characteristics of the interatomic interactions by using an environment-dependent quasiatomic minimal basis set to parameterize the electronic Hamiltonian and overlap matrices of the system. The TB potential accurately describes *sp*, sp^2 and sp^3 chemical bonding in carbon on an equal footing and has been demonstrated to exhibit excellent accuracy and transferability for various crystalline structures and liquid phase of carbon in several previous publications [18-22]. It has been shown that the 3c TB model used in our simulations has the accuracy comparable to that of DFT while about 2 to 3 order of magnitude faster. In particular, the pair-correlation functions $g(r)$ and the static structure factors $S(Q)$ of the liquid carbon at the density of 1.7g/cm^3, 2.6 g/cm^3 [see Fig. 1 of Ref. 22], 2.9 g/cm^3 [see Fig. 8 of Ref. 18] and 3.2g/cm^3 [see Fig.1 of Ref. 22] and temperature of 5000K obtained from our TBMD simulations are in very good agreement with those from the first-principles MD simulations. This good agreement ensures the reliability of the TBMD calculation results. The TBMD simulation to generate *a-Dia* structure is performed with 512 carbon atoms in a cubic supercell and with periodic boundary conditions. Only the Γ point is used for the electronic structure calculations. The MD simulations are performed at

constant volume and constant temperature (i.e., NVT ensemble) and the time step is 1.4 fs. At each temperature, the temperature of the system is controlled by using a stochastic temperature control method to initialize the velocities of the atoms for 2000 MD steps, and then switch to the velocity scaling for temperature control. Initially, four liquid carbon samples with densities of 3.3, 3.4, 3.5, and 3.6 g/cm^3, respectively, are equilibrated at 5000 K. The four systems are then quenched down to 0 K by a stepped cooling procedure in which the temperature of the system is reduced by 500 K at a time and the TBMD simulation is performed for 10,000 steps at each temperature. The volume and shape of the MD cells are kept unchanged in the cooling process. The four quenched samples at T=0 K are then relaxed to the local energy minima and zero pressure by a steepest-descent procedure.

TABLE 1. The densities, fractions of 3- and 4-folded atoms, and bulk moduli of the four TBMD-generated *a-Dia* structures.

Sample	Initial density (g/cm^3)	Final density (g/cm^3)	3-folded fraction	4-folded fraction	Bulk modulus (GPa)
1	3.3	3.30	4.6%	95.4%	435
2	3.4	3.30	3.4%	96.6%	447
3	3.5	3.30	4.7%	95.3%	430
4	3.6	3.39	2.6%	97.4%	435

The four *a-Dia* structures obtained in this way all have high fraction (over 95%) of fourfold-coordinated atoms and have the density between 3.3 to 3.4 g/cm^3. More information of these four *a-Dia* samples is listed in Table 1. We note that the cooling rates have a significant influence on the structural order of amorphous materials. A few percent of 3-folded "defects" in our *a-Dia* samples is likely due to the fast cooling rate (~10^{13} K/s) in the MD simulations. We estimate the bulk moduli of these *a-Dia* structures through the Murnaghan's equation of state fitting to the energy-volume (E-V) curves calculated by our TB method at T = 0 K [23]. These values are in the range of 430-447 GPa as shown in Table 1. The bulk modulus of crystalline diamond from the same TB potential is 498 GPa. Therefore, the generated *a-Dia* can also be considered as ultra-high incompressible solids as their bulk moduli reach about 87% of the bulk modulus of crystalline diamond. In Ref. [1], the density of the *a-Dia* sample is estimated to be 3.3 ± 0.1 g/cm^3 and the percentage of tetrahedral bonding is reported to be close to 98%. We note that the *a-Dia* structure obtained by our TBMD simulation with the initial liquid density of 3.6 g/cm^3 has the highest fraction (97.4%) of fourfold-coordinated atoms. The final density of this sample is 3.39 g/cm^3. In the following, the property analysis is based on this sample

unless otherwise specified. In addition, we also note that in Table 1, the sample 2 has a higher bulk modulus but a lower fraction of 4-folded coordinated carbon atoms, compared to sample 4. This abnormal result indicates that the bulk modulus of *a-Dia* not only dependents on the percentage of 4-folded coordinated sites in the sample, but also on the details of the atomic packing at these sites.

III. Results and Discussion

A. Structural Properties

Fig. 1 displays the pair-correlation function g(r), the static structure factor S(Q), and the bond-angle distribution function P(θ) of the *a-Dia* sample, respectively. These structural properties are averaged over 10,000 MD steps at T=700 K, after 2,000 MD steps of equilibration at this temperature. In order to simulate the system at a given temperature T with quantum correction, the MD temperature T_{MD} is determined by requiring the mean kinetic energy of the system in the MD simulation to be same as that of the corresponding quantum system at temperature T (including zero-point motion),

$$T_{MD} = \frac{1}{k_B}\int h\nu D(\nu)\left[\frac{1}{2}+\frac{1}{\left(e^{h\nu/k_B T}-1\right)}\right]d\nu, \quad (1)$$

where $D(\nu)$ is the phonon density of states of system [24, 25]. According to the Eq. (1), the TBMD simulations are performed at 700 K to mimic the system at room temperature (300 K) by taking into the effects of zero point-motion of the carbon atoms. The first peak of g(r) is at 1.53 Å, which is slightly smaller than the nearest neighbor distance of the sp^3 bonding crystalline diamond (1.54 Å). There is a gap between the first and second peak of g(r), which is quite different from that of liquid carbon at the same density [22]. The minimum between the first and second peaks in g(r) is about 1.85 Å, which is used as the cutoff distance to determine the coordination number of each site and bond-angle distribution function. The second peak of g(r) around 2.46 Å is also slightly shifted towards smaller distance compared to that of the crystalline diamond (2.52 Å). A shoulder around 2.9 Å in g(r) can be observed in our TBMD simulations, which is much weaker than the third main peak of g(r) of the crystalline diamond. The lack of the fourth and fifth main peaks of g(r) compared to the crystalline diamond indicates that the *a-Dia* has no long-range order. In the static structure factor S(Q) shown in Fig. 1 (b), strong first and second peaks at 3.0 and 5.5 $Å^{-1}$ can be seen. Several well defined peaks at large Q values can also be clearly observed. As for the bond-angle distribution shown in Fig. 1(c), the main peak in P(θ) is sharp and almost centered at the tetrahedral angle 109.5°, which suggest a strong tetrahedral amorphous carbon network.

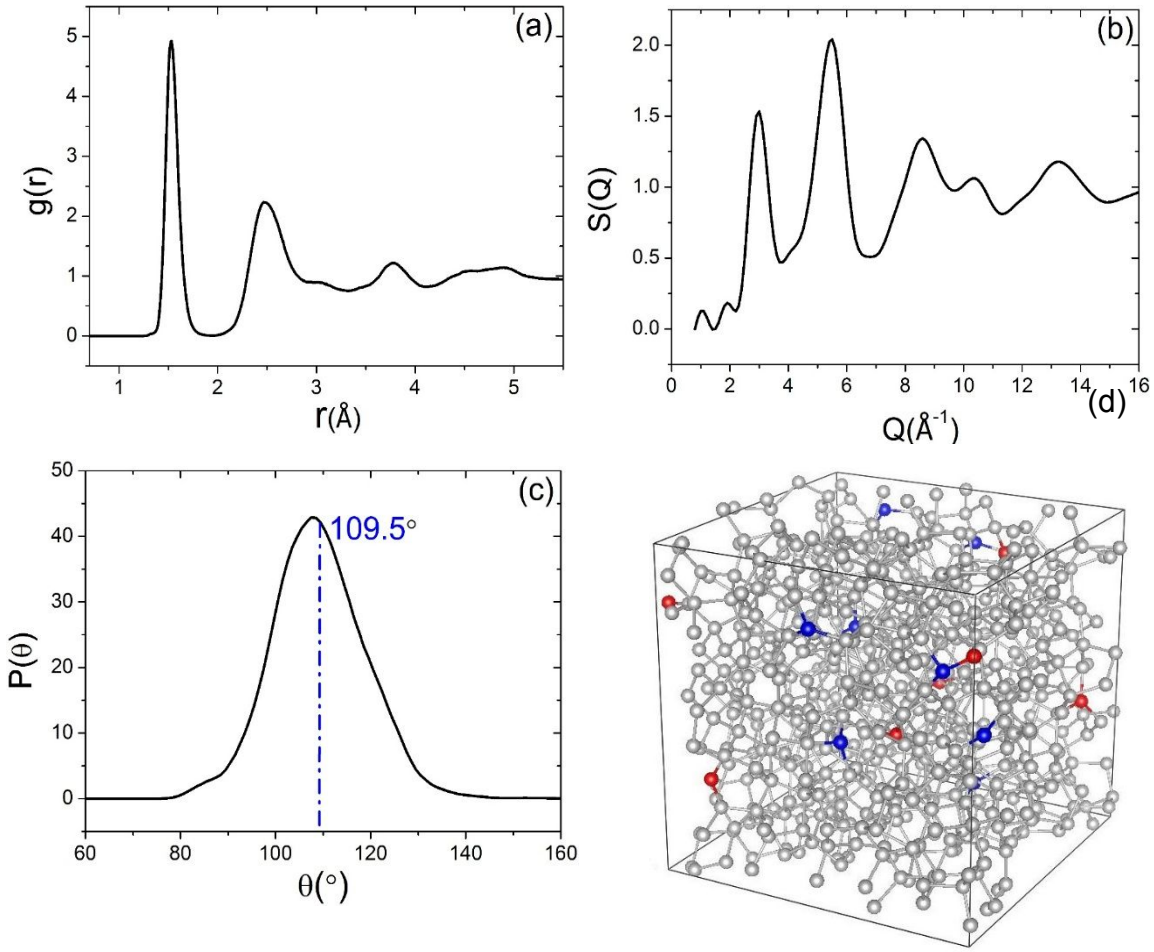

Figure 1. (Color online) (a) Pair-correlation function *g*(r), (b) Static structure factor S(Q), (c) Bond-angle distribution function P(θ), and (d) A representative structural model of the TBMD-generated *a-Dia*. The blue vertical dash dot line in (c) indicates perfect tetrahedral bond angle 109.5°. The light grey balls in (d) denote the sp^3-bonded carbon atoms. The blue and red balls in (d) denote the sp^2-bonded defect atoms with negative and positive charges states, respectively.

Defects in amorphous semiconductors and their effects on the electronic properties of the amorphous materials have been the subjects of intensive investigations in the past several decades. It has been reported that in *a-Si*, the point defects can be either 3-fold coordinated silicon atoms (dangling bonds) or 5-fold coordinated silicon atoms (floating bonds) [26]. In the *a-Dia* structures generated by our TBMD simulations, a few percent of 3-fold coordinated carbon atoms are present and no 5-fold coordinated carbon atom has been observed. The 3-folded defect atoms distribute almost randomly throughout the 4-folded amorphous network as shown by the atoms in color in Fig. 1(d). More details of the atomic structure around these 3-folded defects in the *a-Dia* are plotted in Fig. 2. We find that most of the 3-coordinated defects are associated with 5-membered or 7-membered rings. The presence

of such 3-folded defects has pronounced effects on the electronic properties of the *a-Dia* which are discussed in the following.

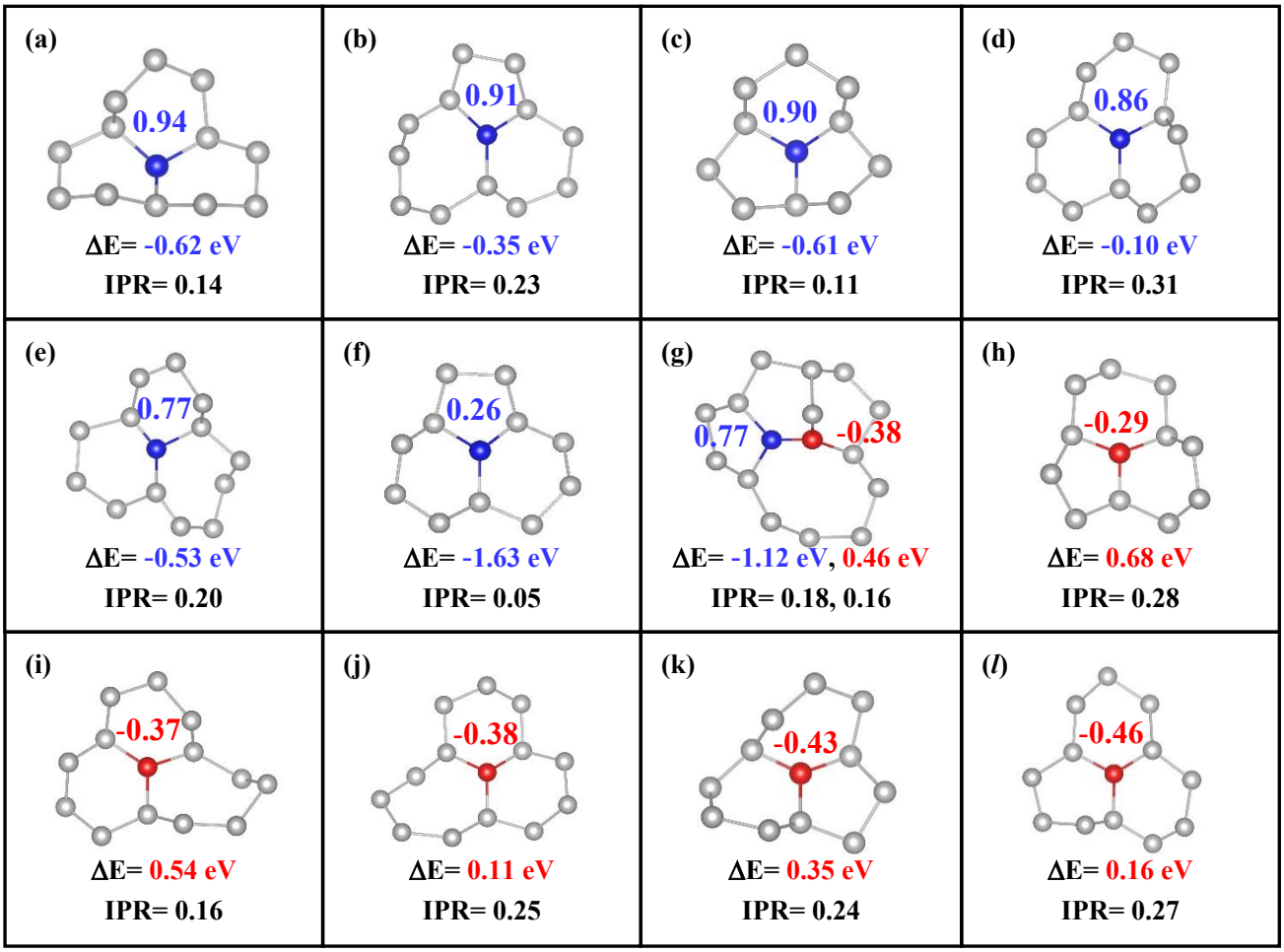

Figure 2. (Color online) The coordination environment of each sp^2-bonded defect atom in the *a-Dia* sample. The blue and red balls denote the sp^2-bonded defect atoms with negative or positive charge states, respectively. The blue and red numbers next to the defect atoms denote the electron gain or loss Δq_i ($\Delta q_i = q_i - 4.0$) on the defect atoms. The light grey balls denote the sp^3-bonded carbon atoms. IPR denotes the localization degree of the electronic states. The electronic gap states with IPR more than 0.1 are essentially localized. The sp^2-bonded defect atoms are the centers of these localized electronic gap states as indicated by the IPR values. The energies of these localized gap states (ΔE, with respected to the Fermi level) are also given.

B. Electronic and Vibrational Properties

Electronic density-of-states (DOS) of the *a-Dia* sample is calculated and plotted in Fig. 3(a). It can be seen that the *a-Dia* structure also has a large band gap similar to that of diamond, except that

there exist some states in the gap region. These gap states are well localized and can be attributed to the presence of threefold coordination defects in the *a-Dia* sample [9, 27]. This can also be seen from the inverse participation ratio (IPR) analysis of the electronic states shown in Fig. 3(b). The IPR of the i^{th} electronic state (eigenvalue) is defined as

$$\mathrm{P}(i) = \sum_{j=1}^{3N} [\mathrm{u}(i,j)\cdot \mathrm{u}(i,j)]^2 \left[\sum_{j=1}^{3N} \mathrm{u}(i,j)\cdot \mathrm{u}(i,j) \right]^{-2}, \quad (2)$$

where N is the number of atoms in the system, and u(i, j) is the normalized $4N$-dimensional (j=1,2, …,$4N$) eigenvector corresponding to the i^{th} eigenvalue. By this definition, the delocalized state will have a small value of IPR while localized state have larger value. IPR equal to 1 if the state is localized only on one atom. From the plot shown in Fig. 3(b), we can see that the states in the gap have large IPR and thus well localized. We find that the gap states with IPR more than 0.1 are essentially localized on the 3-folded defect atoms as shown in Fig. 2.

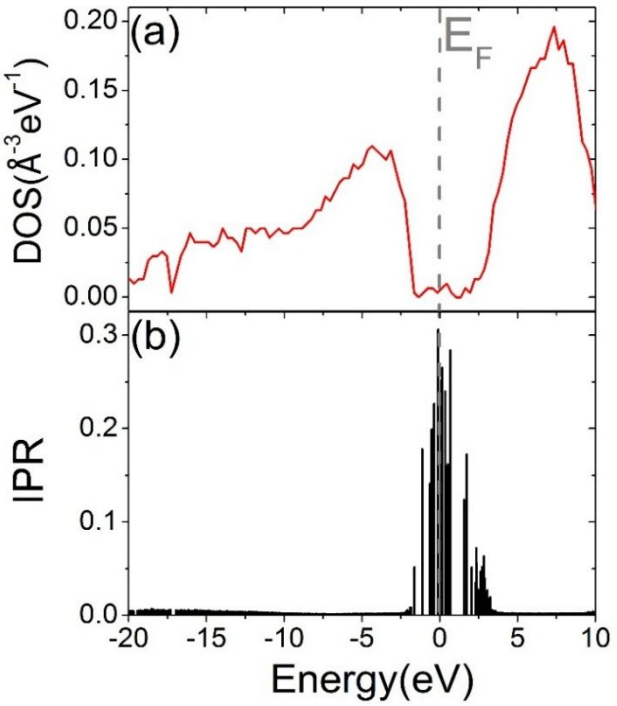

Figure 3. (Color online) (a) Electronic density-of-states (DOS) from the 3c-TB calculation for the TBMD-generated 512-atom *a-Dia* sample. (b) Inverse participation ratios (IPR) of the electronic state in the *a-Dia* sample. The Fermi level is set to 0.0 eV.

We also calculate the amount of electron q_i on each atom in the *a-Dia* sample by Mulliken charge analysis based on the electronic structures of the *a-Dia* from our TB calculations [19]. We find that

most of the carbon atoms in the *a-Dia* have the atomic charge very close to 4.0 electrons, the valence electrons of a neutral carbon atom. The variations of the electron charge around its neutral atomic charge value, i.e., $\Delta q_i = q_i - 4.0$, are calculated. It is interesting to note that the carbon atoms having noticeable electron charge variations Δq_i are the 3-coordinated defect atoms. In comparison, more than 99% of 4-folded atoms has $|\Delta q_i|$ less than 0.1. We find that the 3-folded carbon atoms in the *a-Dia* sample can be either electron acceptors or donators. Therefore the charge states of these defects can be either negative ($0.26 < \Delta q_i < 0.94$) or positive ($-0.46 < \Delta q_i < -0.29$) depending on their local bonding topologies and configurations as shown in Fig. 2. From Fig. 2(*a*) to 2(*l*), the Δq_i on the sp^2-bonded defect carbon atom gradually goes from positive to negative, indicating that the defect changes from negatively-charged defect (blue balls in Fig. 2 (*a*)-(*g*)) to positively-charged defect (red balls in Fig. 2 (*g*)-(*l*)). It is interesting to note that in Fig. 2 (g), two 3-folded defects are connected to each other. One defect is negatively charged while another is positively charged. From the IPR analysis discussed above, we find that the gap states below the Fermi level are localized on those 3-folded atoms with negative charge states, while the gap states above Fermi level are localized on the positively charged 3-folded defect atoms. The energies of the gap states relative to Fermi level are shown by ΔE in Fig. 2.

The vibrational properties of the *a-Dia* have also been investigated by our TB calculations at T=0 K. Finite atomic displacement method has been used to numerical calculate the 1536×1536 force constant matrix for our 512-atom *a-Dia* sample. Similar calculation has also been performed for a 512-atom crystalline diamond structure for comparison. In Fig. 4(a) and (b), we show the vibrational density-of-states of the crystalline diamond and that of the TBMD-generated *a-Dia* sample. It can be seen that the vibrational spectrum of the *a-Dia* contains two major broad peaks around 21 and 36THz, respectively. In comparison with that of the crystalline diamond structures, the vibrational spectrum of the *a-Dia* exhibits extra intensities at frequencies beyond the highest vibrational frequency (42THz) of the crystalline diamond. In order to gain further insight into these extra high frequency modes which are absent in crystalline diamond structure, we performed detailed analysis for these extra modes. The degree of localization for a vibrational mode can also be characterized by its inverse participation ratio IPR, similar to the calculation for the electronic state localization discussed above [27, 28]. As shown in Fig. 4(c), the vibrational modes ranging from 8 to 42THz are considerably extended, whereas the high-frequency modes (from 42 to 56THz) and a few low-frequency modes (from 6 to 9THz) are strongly localized. By looking into which atoms the high-frequency modes are localized on, we find that each of these modes are mainly localized on pairs of atoms which tend to have bond length much shorter than the normal bond lengths in crystalline structures. These atoms include 1 pairs of 3-folded atoms, 21 pairs of 4-folded atoms and 6 pairs mixed 4 and 3 coordinated atoms, respectively. The

bond-length strains for these atoms in comparison with those of the other atoms in the *a-Dia* sample are shown in Fig. 4(d). The bond-length strain is defined as $(d - d_0)/d_0$, where d is the bond length

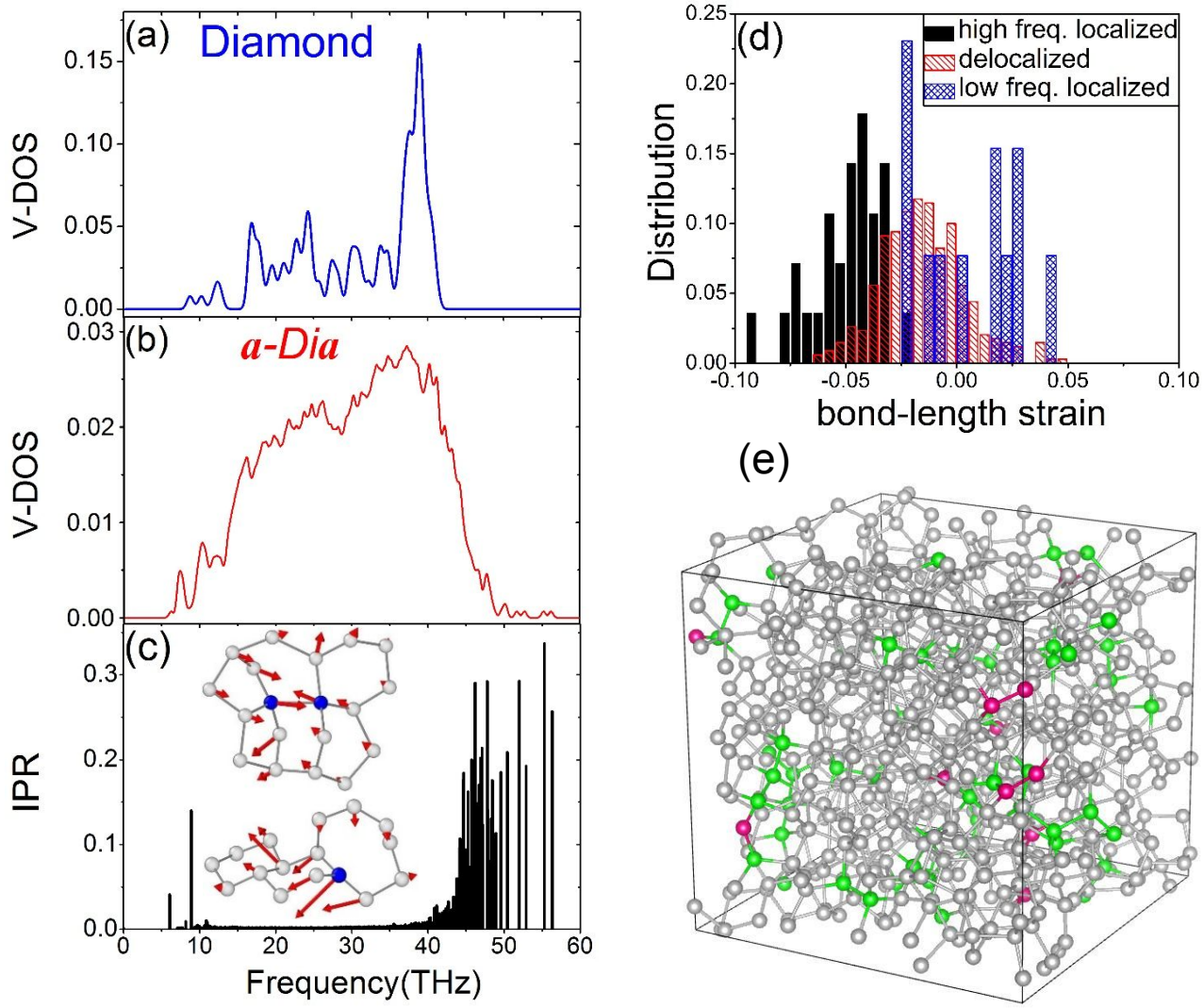

Figure 4. (Color online) Vibrational density-of-states (V-DOS) calculated with 3c-TB potential for (a) crystalline diamond in a supercell containing 512 atoms and (b) the TBMD-generated 512-atom *a-Dia* sample. (c) Inverse participation ratios of the vibrational modes in the *a-Dia* sample. The inset in (c) shows the eigenvectors of the two localized modes at the low frequencies of 6.1 THz (upper) and 8.9 THz (lower), respectively. The amplitudes of the blue balls have been rescaled by a factor of 0.5 for the 6.1 THz mode and 0.3 for the 8.9 THz mode for a better visualization. (d) Distributions of bond-length strain of the carbon atoms involved in the localized and delocalized vibrational modes, respectively. (e) The structure model of the TBMD-generated *a-Dia* sample where the atoms associated with the localized vibrational modes (with IPR > 0.10) are shown in colors. The magenta balls denote the sp^2-bonded carbon atoms while the green balls denote the sp^3-bonded carbon atoms

related to localized vibrational modes.

between two atoms and d_0 takes the values of 1.54, 1.42, and 1.48 Å for a pair of 4-4 folded, 3-3 folded and mixed 4-3 folded atoms, respectively. It is clearly shown that the pair of atoms which localizes the high-frequency modes tend to have shorter bond length (more negative strain). This bond-length strain distribution is understandable since shorter bond is stiffer and thus leads to higher vibration frequency.

On the other hand, the atoms associated with the two localized vibrational modes at the low frequencies of 6.1 THz and 8.9 THz have significantly longer bond lengths as one can see from Fig. 4 (d). These two low frequency modes are localized on two small clusters respectively in the *a-Dia* sample as shown in the inset of Fig. 4 (c) where the vibrational eigenvectors of these two modes are presented. The 6.1 THz mode has large amplitudes on 2 atoms (the balls in blue) which form a weak bond with the bond length 1.81Å among them (not shown in Fig. 4 (d)). These two atoms move towards the opposite direction and bring the rings on each side of the cluster to move with them. This low-frequency mode can be considered a squeeze mode. The 8.9 THz mode is strongly localized on one atom (in blue) which has the largest amplitude. The eigenvectors of this mode show that the directions of atomic displacements in the cluster rotate gradually, forming a kind of twisting mode.

The spatial distribution of the carbon atoms associated with the localized vibrational modes in the *a-Dia* sample is shown in Fig. 4(e). The magenta balls denote the sp^2-bonded carbon atoms related to localized vibrational modes, while the green balls denote the sp^3-bonded carbon atoms related to localized vibrational modes. It can be seen that the atoms involved in the localized vibrations are randomly distributed throughout the *a-Dia* sample, and most of these are 4-folded atoms.

IV. Conclusion

In summary, with the efficiency and accuracy of the three-center TBMD simulations, we have generated a realistic *a-Dia* structure and studied the structural, electronic, and vibrational properties of the *a-Dia* sample. Our calculation results show that *a-Dia* structures with more than 97% of sp^3 bonding fraction and with an ultra-high incompressibility similar to that of crystalline diamond can be achieved. The point defects in *a-Dia* are predominately 3-coordinated carbon atoms which introduce localized electronic states in the gap otherwise the *a-Dia* would have a wide gap similar to that of crystalline diamond. We also show that large local strain in the *a-Dia* network produces well localized vibrational modes, most of them with frequencies higher than highest vibration frequency in crystalline diamond. The presence of the localized electronic states and vibrational modes in a-*Dia* would act as scattering centers for the electrons and phonons, which would lead to the reduction of the mean free

paths of electron and phonons and affect the electron transport and thermal conductivity in the *a-Dia*. This would be an interesting subject for further investigations.

Conflict of Interest

There are no conflicts of interest to declare.

Acknowledgments

This work was supported by the U.S. Department of Energy (DOE), Office of Science, Basic Energy Sciences, Materials Science and Engineering Division including a grant of computer time at the National Energy Research Scientific Computing Centre (NERSC) in Berkeley, CA. Ames Laboratory is operated for the U.S. DOE by Iowa State University under Contract No. DE-AC02-07CH11358. Rong Cheng and Wen-Cai Lu were also supported by the National Natural Science Foundation of China (Grant No. 21773132).

References

[1] Z. D. Zeng, L. X. Yang, Q. S. Zeng, H. B. Lou, H. W. Sheng, J. G. Wen, D. J. Miller, Y. Meng, W. G. Yang, W. L. Mao, and H.-K. Mao, *Nat. Commun.* 2017, 8, 322.

[2] T. B. Shiell, D. G. McCulloch, D. R. McKenzie, M. R. Field, B. Haberl, R. Boehler, B. A. Cook, C. de Tomas, I. Suarez-Martinez, N. A. Marks, and J. E. Bradby, *Phys. Rev. Lett.* 2018, 120, 215701.

[3] J. Schwan, S. Ulrich, H. Roth, H. Ehrhardt, S. R. P. Silva, J. Robertson, R. Samlenski, and R. Brenn, *J. Appl. Phys.* 1996, 79, 1416.

[4] A. LiBassi, A.C. Ferrari, V. Stolojan, B.K. Tanner, J. Robertson, and L.M. Brown, *Diam. Relat. Mater.* 2000, 9, 771.

[5] Y. Lin, L. Zhang, H.-K. Mao, P. Chow, Y. M. Xiao, M. Baldini, J. F. Shu, and W. L. Mao, *Phys. Rev. Lett.* 2011, 107, 175504.

[6] G. Galli, R. M. Martin, R. Car, and M. Farrinello, *Phys. Rev. Lett.* 1989, 62, 555.

[7] N. A. Marks, D. R. McKenzie, B. A. Pailthorpe, M. Bernasconi, and M. Parrinello, *Phys. Rev. B*: *Condens. Matter Mater. Phys.* 1996, 54, 9703.

[8] D. G. McCulloch, D. R. McKenzie, and C. M. Goringe, *Phys. Rev. B*: *Condens. Matter Mater. Phys.* 2000, 61, 2349.

[9] J. C. Han, W. Gao, J. Q. Zhu, and S. H. Meng, *Phys. Rev. B*: *Condens. Matter Mater. Phys.* 2007, 75, 155418.

[10] M. A. Caro, R. Zoubkoff, O. L. Acevedo, and T. Laurila, *Carbon* 2014, 77, 1168.

[11] N. A. Marks, N. C. Cooper, D. R. McKenzie, D. G. McCulloch, P. Bath, and S. P. Russo, *Phys.*

Rev. B: *Condens. Matter Mater. Phys.* 2002, 65, 075411.

[12] C. D. Tomas, I. S. Martinez, and N. A. Marks, *Carbon* 2016, 109, 681.

[13] C. Z. Wang, K. M. Ho, and C. T. Chan, *Phys. Rev. Lett.* 1993, 70, 611.

[14] T. Frauenheim, P. Blaudeck, U. Stephan, and G. Jungnickel, *Phys. Rev. B*: *Condens. Matter Mater. Phys.* 1993, 48, 4823.

[15] B. R. Djordjević, M. F. Thorpe, and F. Wooten, *Phys. Rev. B*: *Condens. Matter Mater. Phys.* 1995, 52, 5685.

[16] M. A. Caro, V. L. Deringer, J. Koskinen, T. Laurila, and G. Csányi, *Phys. Rev. Lett.* 2018, 120, 166101.

[17] B. Bhattarai, A. Pandey, and D. A. Drabold, *Carbon* 2018, 131, 168.

[18] W.-C. Lu, C. Z. Wang, L.-Z. Zhao, W. Qin, and K. M. Ho, *Phys. Rev. B*: *Condens. Matter Mater. Phys.* 2015, 92, 035206.

[19] W. Zhang, W.-C. Lu, H.-X. Zhang, K.M. Ho, and C.Z. Wang, *Carbon* 2016, 110, 330.

[20] W. Zhang, W.-C. Lu, H.-X. Zhang, K. M. Ho, and C. Z. Wang, *J. Phys.: Condens. Matter* 2016, 28, 115001.

[21] W. Zhang, M. Kim, R. Cheng, W.-C. Lu, H.-X. Zhang, K. M. Ho, and C. Z. Wang, *J. Phys. Chem. C* 2020, 124, 2370.

[22] R. Cheng, W.-C. Lu, K. M. Ho, and C. Z. Wang, *Phys. Chem. Chem. Phys.* 2020, 22, 14630.

[23] V. G. Tyuterev, N. Vast, *Computational Materials Science* 2006, 38, 350.

[24] H. C. Andersen, *J. Chem. Phys.* 1980, 72, 2384.

[25] C. Z. Wang, C. T. Chan, and K. M. Ho, *Phys. Rev. B*: *Condens. Matter Mater. Phys.* 1990, 42, 11276.

[26] Pantelides S. T., *Phys. Rev. Lett.* 1986, 57, 2979-2982.

[27] C. Z. Wang, and K. M. Ho, *Phys. Rev. Lett.* 1993, 71, 1184.

[28] J. H. Zhang, C. Z. Wang, Z. Z. Zhu, and V. V. Dobrovitski, *Phys. Rev. B*:*Condens. Matter Mater. Phys.* 2011, 84, 035211.